Sensors and Materials, Vol. 37, No. 12 (2025) 5577–5584
MYU Tokyo

S & M 4264

Tunable Emission and Stability of $MAPbI_3$ Nanocrystals by Room-temperature Ligand-assisted Reprecipitation with Nonpolar Solvent

Juin J. Liou,[1] Yu-Sen Huang,[2] Tzu An Ho,[2] and Chien-Jung Huang[2*]

[1]College of Electronic and Information Engineering, Shandong University of Science and Technology, Qingdao, Shandong Province, China
[2]Department of Applied Physics, National University of Kaohsiung, Kaohsiung City 811726, Taiwan (ROC)

(Received November 25, 2025; accepted December 16, 2025)

Keywords: $MAPbI_3$ nanocrystals, average lifetime, diethyl ether, room-temperature synthesis, tunable emission, blue shift

In this paper, we present an innovative room-temperature ligand-assisted reprecipitation (LARP) strategy, in which the introduction of diethyl ether plays a crucial role in the synthesis of $MAPbI_3$ nanocrystals. Diethyl ether is a weakly polar solvent. Its introduction regulates nucleation and early-stage crystal growth. As a result, enhanced homogeneous nucleation and smaller nanocrystals are obtained. By tuning solvent polarity and optimizing the precursor-to-antisolvent ratio, the addition of diethyl ether not only reduces crystal size and enhances the quantum confinement effect, thereby inducing a pronounced spectral blue shift and enabling emission tunability across the 500–700 nm range, but also suppresses lattice defect formation and passivates surface states, effectively minimizing nonradiative carrier recombination. Consequently, the incorporation of diethyl ether markedly prolongs the average carrier lifetime, improves precursor solution stability, and enhances the overall durability of the nanocrystals, achieving stable light emission. This approach significantly expands the potential of $MAPbI_3$ nanocrystals in optoelectronic applications and provides an effective pathway toward multicolor-tunable and long-term stable light emission.

1. Introduction

Organic–inorganic hybrid perovskites $MAPbX_3$ (X = Cl, Br, I) have attracted significant attention in recent years as luminescent materials owing to their excellent optoelectronic properties, including high absorption coefficients, small exciton binding energies, high carrier mobilities, tunable direct optical bandgaps, and low-cost room-temperature processing.[1–3] In the synthesis of perovskite quantum dots via the ligand-assisted reprecipitation (LARP) method, most previous studies were focused on improving the stability of red-emitting $MAPbI_3$ nanocrystals, whereas reports on short-wavelength, small-size $MAPbI_3$ nanocrystals remain

*Corresponding author: e-mail: chien@nuk.edu.tw
https://doi.org/10.18494/SAM6083

ISSN 0914-4935
https://myukk.org/

limited. Here, we aim to fabricate short-wavelength $MAPbI_3$ nanocrystals to advance their potential in optoelectronic applications. Diethyl ether, a weakly polar solvent, has been demonstrated to enhance crystallinity and reduce defect density in perovskite thin films;[4] however, its direct incorporation into $MAPbI_3$ nanocrystal precursor solutions has not been explored. In this work, diethyl ether was employed as a key solvent in synthesizing short-wavelength $MAPbI_3$ nanocrystals, and its effects were systematically compared in two nonpolar solvents, chlorobenzene (CB) and chloroform (CF), to investigate the influence of solvent conditions on nanocrystal optical properties and stability. Using LARP, the nucleation and growth of $MAPbI_3$ nanocrystals were tuned by varying the solvent polarity, and consistent with previous reports,[5] lower-polarity nonpolar solvents were expected to yield shorter photoluminescence (PL) wavelengths. The effects of CB and CF on nanocrystal emission and structure were compared, followed by the evaluation of the changes induced by diethyl ether addition. This approach enables the assessment of whether diethyl ether, as a weakly polar modifying solvent, can effectively suppress defects, prolong carrier lifetimes, and produce $MAPbI_3$ nanocrystals with tunable emission and enhanced stability, providing a foundation for future optoelectronic applications.

2. Materials and Methods

2.1 Materials

The precursor solution for $MAPbI_3$ quantum dots (QDs) was prepared by dissolving methylammonium iodide (MAI, 99.99%, Ruil Long Optical) and lead iodide (PbI_2, 99.9985%, Thermo Scientific) in a mixed solvent of acetonitrile (ACN, ≥99.5%, Sigma-Aldrich), diethyl ether (DEE, ≥99.0%, J.T. Baker), oleic acid (OA, 97%, Acros Organics), and oleylamine (OLM, 80–90%, Sigma-Aldrich). Chlorobenzene (CB, ≥99.5%, Fluka Analytical) and chloroform (CF, ≥99.8%, Fisher Chemical) were used as antisolvents for the formation of $MAPbI_3$ QDs.

2.2 Synthesis of MAPbI3 precursor

To prepare the $MAPbI_3$ QD solution, the LARP method was employed, as shown in Fig. 1. First, solid precursors of MAI (15.9 mg) and PbI_2 (46.1 mg) were dissolved in 2 mL of ACN. Subsequently, 50 μL of DEE, the key solvent in this experiment, 200 μL of OA, and 200 μL of OLM were added as ligands. The mixture was vigorously stirred at room temperature at a speed of 550 rpm for 2 h to promote uniform mixing of the reactants, prevent aggregation, and ensure the formation of a homogeneous liquid precursor for consistent nucleation and growth. The stirring rate can influence the particle size; higher stirring speeds generally lead to smaller nanoparticles owing to faster nucleation. The carboxylic group in OA prevents $MAPbI_3$ aggregation through steric hindrance, whereas the amine group in OLM participates in the regulation of $MAPbI_3$ crystallization. These ligands possess long alkyl chains and polar functional heads that can bind to atoms or ions on the $MAPbI_3$ surface, thereby stabilizing the nanocrystals. During the stirring process, the initially milky-white precursor gradually turned into a yellow solution.

2.3 Synthesis of $MAPbI_3$ nanocrystals

We added 100 μL of the precursor solution into 10 mL of a nonpolar solvent, either CF or CB, and stirred the mixture at 550 rpm to prepare smaller and more stable $MAPbI_3$ nanocrystals, as shown in Fig. 1. If the precursor concentration is too high, rapid aggregation may occur in the antisolvent, leading to the formation of large nanocrystals or nonemissive byproducts. Therefore, precisely controlling the ratio between the precursor and the nonpolar solvent is crucial.

3. Results and Discussion

3.1 TEM analysis

As illustrated in Figs. 2(a) and 2(b), discrete and well-dispersed QDs can be observed. When CF is employed as the nonpolar dispersion solvent,[6] its higher polarity hinders precursor

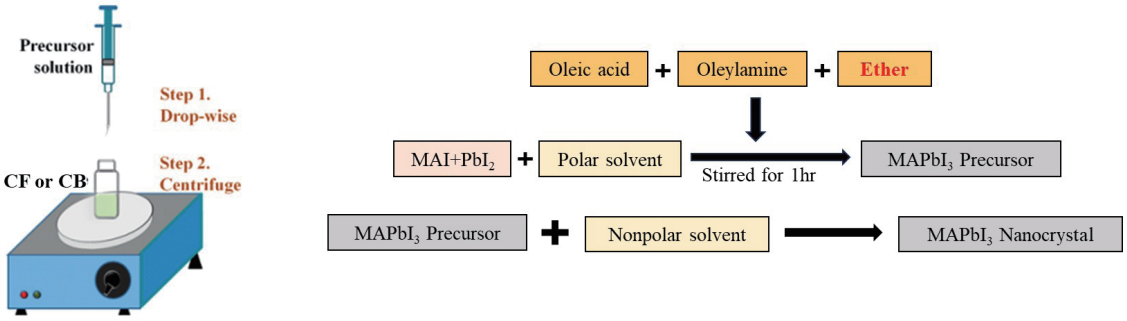

Fig. 1. (Color online) Schematic diagram of $MAPbI_3$ QD solution preparation.

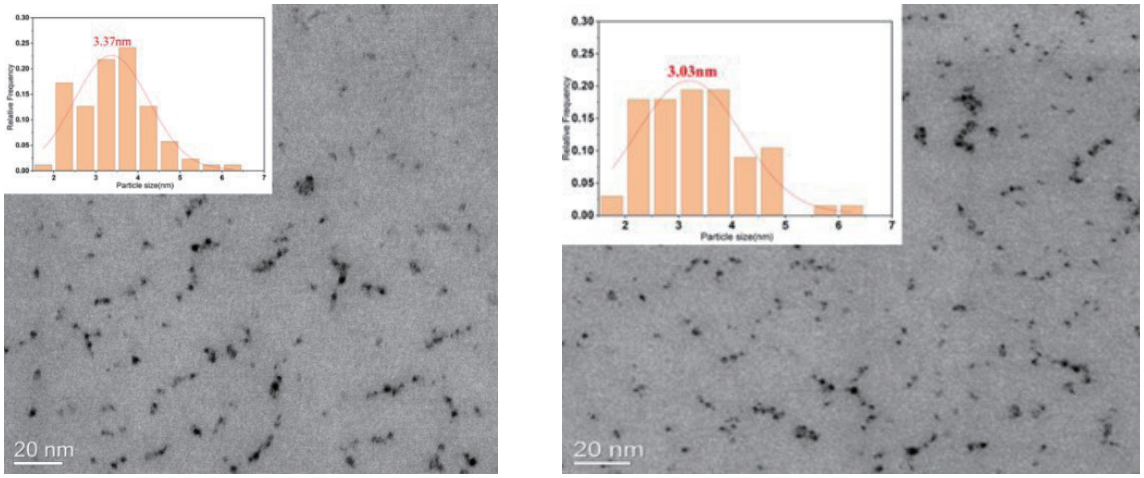

(a) (b)

Fig. 2. (Color online) TEM images of samples prepared using (a) CF without and (b) containing DEE with $MAPbI_3$ QDs, and (c) CB without and (d) containing DEE with $MAPbI_3$ QDs.

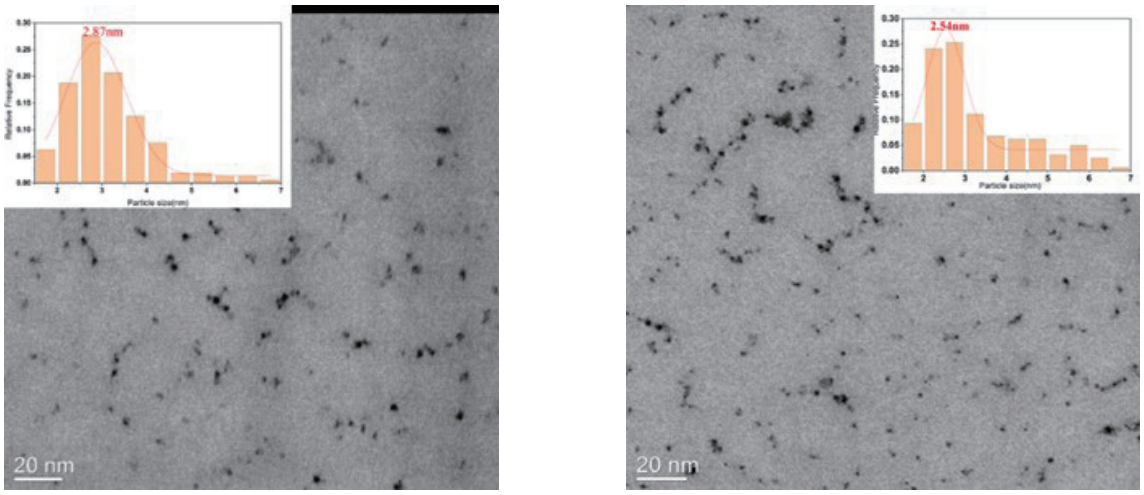

(c) (d)

Fig. 2. (Continued) (Color online) TEM images of samples prepared using (a) CF without and (b) containing DEE with $MAPbI_3$ QDs, and (c) CB without and (d) containing DEE with $MAPbI_3$ QDs.

nucleation, resulting in larger (average: 3.37 nm) QDs. In contrast, using CB as the nonpolar dispersion solvent with its lower polarity facilitates precursor dispersion and nucleation, leading to small (average: 2.87 nm) QDs.

According to Figs. 2(c) and 2(d), the incorporation of DEE, a weakly polar solvent, into the precursor solution decreases the effective solubility of the precursor in CB and CF, thereby increasing the instantaneous supersaturation.[7] This promotes enhanced homogeneous nucleation, ultimately yielding a small average particle size and a narrow size distribution.[8] TEM analysis confirms this effect: for CF, the average particle size decreased from 3.37 to 3.03 nm, corresponding to a reduction of 0.34 nm, whereas for CB, the average particle size decreased from 2.87 to 2.54 nm, a reduction of 0.33 nm. Therefore, the addition of DEE effectively modulates the size characteristics of the nanocrystals, indicating that ether plays a crucial role in regulating nucleation and growth during the LARP synthesis.

3.2 PL analysis

The PL spectra of $MAPbI_3$ QDs synthesized under different precursor and solvent conditions are presented in Figs. 3(a)–3(c). As shown in Fig. 3(a), the PL peak of the CB sample is located at 607 nm, whereas that of the CF sample appears at 620 nm. The emission of the CB sample clearly exhibits a blue shift compared with the CF sample, indicating that the particle size is smaller and the quantum confinement effect is more pronounced in the CB sample than in the CF sample. When the nanocrystal size approaches the exciton Bohr radius, the confinement of charge carriers increases the effective bandgap energy, resulting in shorter emission wavelengths. This phenomenon can be quantitatively explained by the following Brus model.[8]

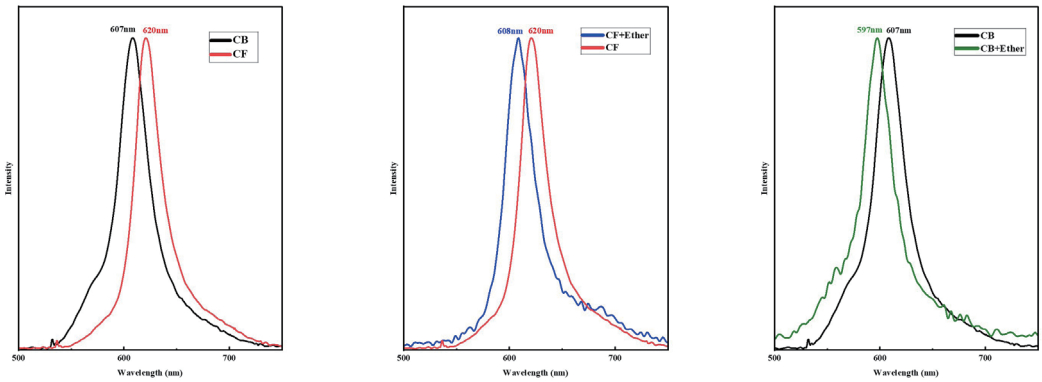

(a) (b) (c)

Fig. 3. (Color online) (a) PL spectra of the CF and CB samples. (b) CF with and without DEE. (c) CB with and without DEE.

$$E_g(d) = E_{bulk} + \frac{3\hbar^2\pi^2}{2m^* d^2} \tag{1}$$

Equation (1) describes the particle size-bandgap relationship, where E_{bulk} is the bulk bandgap, $\hbar$ is Planck's constant, m^* is the effective mass of the carriers, and d is the particle diameter. As d decreases, E_g increases, leading to a notable blue shift in the PL spectrum. This behavior has been reported in other semiconductor nanocrystal systems.[9] In Fig. 3(b), the introduction of DEE during CB sample fabrication (CB + Ether) further shifts the PL peak from 607 to 597 nm, indicating that ether promotes the formation of smaller nanocrystals. This behavior may arise from the high volatility and moderate polarity of ether, which promote nucleation while suppressing grain growth during antisolvent precipitation.[10,11] Consequently, smaller and more uniform $MAPbI_3$ QDs are formed. A similar trend is observed in Fig. 3(c), where the PL peak of CF shifts from 620 nm (CF) to 608 nm (CF + Ether) after ether addition. The consistent blue-shift behavior demonstrates that DEE effectively modulates the crystal size and corresponding electronic structure of $MAPbI_3$ QDs. Its systematic blue shift indicates that both precursor formulation and ether-assisted crystallization jointly influence the QD band structure. These findings are consistent with those of previous studies showing that solvent polarity and crystallization kinetics strongly affect the nucleation and growth of perovskite nanocrystals.[12,13]

Our results suggest that the introduction of ether provides an effective route for tuning the optical emission of $MAPbI_3$ QDs. The enhanced bandgap and blue-shifted emission due to reduced particle size highlight the potential of solvent engineering as a strategy for controlling the optoelectronic properties of perovskite nanocrystals, which is crucial for the optimization of perovskite-based LEDs and photovoltaic devices.[14,15]

3.3 Time-resolved photoluminescence (TRPL) analysis

To further investigate the carrier dynamics and surface defect behavior of different samples, TRPL measurements were performed, as shown in Figs. 4(a)–4(c). TRPL reflects the

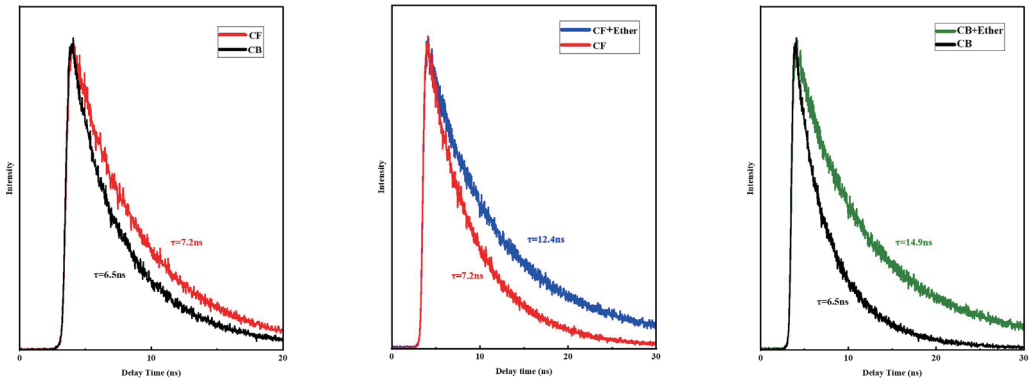

(a) (b) (c)

Fig. 4. (Color online) (a) TRPL lifetime decay curves of the CF and CB samples. (b) CF samples with and without DEE. (c) CB samples with and without DEE.

recombination of carriers returning from the photoexcited state to the ground state and can be used to analyze the difference between radiative and nonradiative recombination rates. The average photoluminescence lifetime can be expressed as[16]

$$\tau = \frac{1}{k_r + k_{nr}}. \tag{2}$$

Equation (2) indicates that the carrier lifetime (τ) is related to the recombination mechanisms within the material, where τ is the measured average carrier lifetime (ns), k_r is the radiative recombination rate (ns^{-1}), and k_{nr} is the nonradiative recombination rate (ns^{-1}). As shown in Fig. 4(a), the CF sample exhibits a longer average lifetime (τ = 7.2 ns) than the CB sample (τ = 6.5 ns), indicating that the former possesses larger grain size and lower surface defect density, resulting in suppressed nonradiative recombination (k_{nr}) and prolonged carrier lifetime. This can be attributed to its superior crystallinity and surface coordination, suggesting that the slower nucleation rate in the CF process facilitates the formation of structurally intact $MAPbI_3$ nanocrystals with fewer I^- vacancies and under-coordinated Pb^{2+} trap centers.[17–19] Further comparison of Figs. 4(b) and 4(c) reveals that introducing DEE into both CB and CF systems significantly enhances their average lifetimes (CB + Ether: τ = 14.9 ns; CF + Ether: τ = 12.4 ns). This indicates that DEE effectively regulates the coordination environment of the precursor solution during synthesis, stabilizes Pb and I bonds, and reduces the surface defect density and nonradiative recombination rate.[20] Because of its high volatility and moderate Lewis basicity, the ether molecule can temporarily coordinate with Pb^{2+}, promoting uniform nucleation and smoother crystal surfaces, thus achieving effective surface passivation.[21]

The TRPL results are consistent with those of the PL spectra and TEM nanocrystal size analysis: as particle size decreases, a blue shift occurs owing to the quantum confinement effect, accompanied by a shortened carrier lifetime caused by increased surface defects. However, upon adding ether, although grain size slightly decreases, the enhanced surface passivation effectively suppresses nonradiative recombination, resulting in a prolonged PL lifetime. This highlights the crucial role of ether in tuning the crystallinity and optical stability of $MAPbI_3$ QDs.

4. Conclusions

In this study, we systematically elucidated the structural and optical modulation induced by DEE during the synthesis of $MAPbI_3$ QDs, supported by comprehensive TEM, PL, and TRPL analyses. TEM observations revealed that ether effectively governs the nucleation kinetics, producing smaller and more uniformly distributed nanocrystals, whereas PL spectra demonstrated enhanced quantum confinement and improved radiative efficiency. The TRPL results further revealed the dynamic role of ether in carrier recombination kinetics. The incorporation of ether transforms the decay profile from a fast single-exponential to a slower multi-exponential behavior, indicating the suppression of carrier trapping and re-emission processes associated with surface defect states. This implies that ether reorganizes the surface coordination environment, reduces trap-state density, and stabilizes the electronic band alignment, thereby improving carrier transport pathways and minimizing nonradiative recombination losses.

In summary, DEE functions as both a crystallization modulator and a defect passivation agent. It simultaneously enhances quantum confinement through size control and improves the surface electronic landscape by mitigating defect-induced recombination. These dual effects collectively promote the optical stability and carrier lifetime of $MAPbI_3$ QDs, offering a promising strategy for the development of efficient and durable perovskite QD optoelectronic devices.

Acknowledgments

The authors thank Hao-Chen Chiu, Yuan-Hao Li, and Wei-Jia Luo of the Department of Applied Physics, National University of Kaohsiung (NUK), for their contributions to experiments and data analysis. Financial support from the National Science and Technology Council (NSTC) (Project No. 113-2221-E-390-012) is gratefully acknowledged. The authors also thank the Department of Materials and Optoelectronic Science, National Sun Yat-sen University (NSYSU), for providing access to TEM measurements

References

1 Y. H. Kim, G. H. Lee, Y. T. Kim, C. Wolf, H. J. Yun, W. Kwon, C. G. Park, and T. W. Lee: Nano Energy **38** (2017) 51. https://doi.org/10.1016/j.nanoen.2017.05.002
2 Q. Li, H. Li, H. Shen, F. Wang, F. Zhao, F. Li, X. Zhang, D. Li, X. Jin, and W. Sun: ACS Photonics **4** (2017) 2504. https://doi.org/10.1021/acsphotonics.7b00743
3 C. Liu, Z. Qiu, W. Meng, J. Chen, J. Qi, C. Dong, and M. Wang: Nano Energy **12** (2015) 59. https://doi.org/10.1016/j.nanoen.2014.12.004
4 H. Wang, L. Chen, X. Zhang, Y. Guo, Z. Li, Z. Wang, and J. Zhang: Thin Solid Films **660** (2018) 81. https://doi.org/10.1016/j.tsf.2018.07.041
5 S. Zhou: RSC Adv. **11** (2021) 28410. https://doi.org/10.1039/D1RA04578D
6 J. Shamsi, A. S. Urban, M. Imran, L. De Trizio, and L. Manna: Chem. Rev. **119** (2019) 3296. https://doi.org/10.1021/acs.chemrev.8b00644
7 J. Enomoto, R. Sato, M. Yokoyama, T. Kimura, N. Oshita, K. Umemoto, S. Asakura, and A. Masuhara: RSC Adv. **12** (2022) 5571. https://doi.org/10.1039/D1RA08887D
8 F. Zhang, S. Huang, P. Wang, X. Chen, S. Zhao, Y. Dong, and H. Zhong: ACS Nano **11** (2017) 4509. https://doi.org/10.1021/acs.chemmater.7b01100

9 B. McKenna, A. Shivkumar, B. Charles, and R. C. Evans: Nanoscale **12** (2020) 11694. https://doi.org/10.1039/D0NR03227A
10 L. E. Brus: J. Chem. Phys. **80** (1984) 4403. https://doi.org/10.1063/1.447218
11 C. B. Murray, D. J. Norris, and M. G. Bawendi: J. Am. Chem. Soc. **115** (1993) 8706. https://doi.org/10.1021/ja00072a025
12 N. Yantara, S. Bhaumik, F. Yan, D. Sabba, H. A. Dewi, N. Mathews, P. P. Boix, H. V. Demir, and S. Mhaisalkar: J. Phys. Chem. Lett. **6** (2015) 4360. https://doi.org/10.1021/acs.jpclett.5b02011
13 S. Ha, R. Su, J. Xing, Q. Zhang, and Q. Xiong: Chem. Sci. **8** (2017) 2522. https://doi.org/10.1039/C6SC04474C
14 J. Song, J. Li, X. Li, L. Xu, Y. Dong, and H. Zeng: Adv. Mater. **28** (2016) 4861. https://doi.org/10.1002/adma.201600784
15 S. D. Stranks and H. J. Snaith: Nat. Nanotechnol. **10** (2015) 391. https://doi.org/10.1038/nnano.2015.90
16 Y. Chen, A. Ren, Z. Yang, T. He, X. Ding, H. Zhang, and L. Zou: Phys. Chem. Chem. Phys. **20** (2018) 9419. https://doi.org/10.1039/C8CP00525G
17 D. W. de Quilettes, S. M. Vorpahl, S. D. Stranks, H. Nagaoka, G. E. Eperon, M. Leijtens, A. Z. Kim, and H. J. Snaith: Science **348** (2015) 683. https://doi.org/10.1126/science.aaa5333
18 N. K. Noel, A. Abate, S. D. Stranks, E. Parrott, V. Burlakov, A. Goriely, and H. J. Snaith: ACS Nano **8** (2014) 9815. https://doi.org/10.1021/nn5036476
19 L. Fu, H. Li, L. Wang, R. Yin, B. Li, and L. Yin: Energy Environ. Sci. **13** (2020) 4017. https://doi.org/10.1039/D0EE01767A
20 F. Zhang, J. Li, X. Li, L. Xu, Y. Dong, and H. Zeng: Adv. Mater. **31** (2019) 1900925. https://doi.org/10.1002/anie.202102360
21 A. A. Zhumekenov, M. I. Saidaminov, M. A. Haque, E. Alarousu, S. P. Sarmah, B. Murali, I. Dursun, X.-H. Miao, A. L. Abdelhady, T. Wu, O. F. Mohammed, and O. M. Bakr: ACS Energy Lett. **1** (2016) 32. https://doi.org/10.1021/acsenergylett.6b00002